Geophysical Journal International

Geophys. J. Int. (2015) **202,** 578–583 doi: 10.1093/gji/ggv180

GJI Geomagnetism, rock magnetism and palaeomagnetism

Critical single-domain grain sizes in elongated iron particles: implications for meteoritic and lunar magnetism

Adrian R. Muxworthy[1] and Wyn Williams[2]

[1]*Department of Earth Science and Engineering, Imperial College London, South Kensington Campus, London, SW7 2AZ, United Kingdom. E-mail: adrian.muxworthy@imperial.ac.uk*

[2]*Grant Institute of Earth Science, University of Edinburgh, Kings Buildings, West Mains Road, Edinburgh, EH9 3JW, United Kingdom*

Accepted 2015 April 23. Received 2015 April 16; in original form 2014 October 7

SUMMARY

Kamacite particles (Fe–Ni, Ni < 5 per cent), are very common in extra-terrestrial materials, such as meteorites. It is normally assumed that for kamacite particles to be reliable recorders of magnetic fields, they need to be magnetically uniform (single domain, SD) and thermally stable. Larger particles subdivide into non-uniform multidomain (MD) magnetic structures that produce weaker magnetic signals, while small SD particles become magnetically unstable due to thermal fluctuations and exhibit superparamagnetic behaviour. In this paper we determine the first micromagnetic calculation of the stable SD range domain-state phase diagram for metallic iron; previous calculations were analytical. There is a significant increase in the critical size for the SD/MD threshold size, for example, for cube-shaped iron particles, the critical SD/MD threshold has now been estimated to be 25 nm, compared to 17 nm for previous estimates. The larger critical SD/MD threshold size for iron, agrees better with previously published nanometric observations of domain state for FeNi particles, then early analytical models.

Key words: Numerical approximations and analysis; Magnetic and electrical properties; Rock and mineral magnetism.

1 INTRODUCTION

Kamacite (Fe–Ni, Ni < 5 per cent) is commonly found to be the dominant magnetic mineral in many different types of meteorites including chondritic meteorites (Weiss *et al.* 2010; Pechersky *et al.* 2012; Gattacceca *et al.* 2014) and lunar rocks (Garrick-Bethell & Weiss 2010). Of particular interest are the kamacite particles found inside dusty olivines in chondrules in unequilibrated chondrites, as they have the potential to carry pristine, pre-accretionary, primary remanent magnetisations (Uehara & Nakamura 2006; Lappe *et al.* 2011; Lappe *et al.* 2013), that is, kamacite is one of the most likely minerals to retain magnetic field intensity information acquired during Solar Nebular formation, because the particles are protected from chemical alteration by the encasing olivine. But for the kamacite particles to retain a meaningful palaeomagnetic signal, it is important that the particles' magnetic remanences are metastable for billions of years. The magnetic state that is metastable longest, is magnetically uniform, and is termed single domain (SD; Fig. 1a). True SD states only occur in ellipsoid shapes; in other shapes, for example, parallelepipeds, the magnetisation is non-uniform in corners leading to flowering (Fig 1a). In this paper, we model parallelepiped structures; we refer to flower structures as SD in this paper, when strictly they are not SD.

When SD particles are smaller than a critical threshold size, they are no longer magnetically stable because thermal energy can easily overcome the energy barrier that otherwise prevents domain switching. Such particles then have superparamagnetic (SP) behaviour (Newell 2006). The magnetisation in larger grains above the SD threshold size, form complex non-uniform or multidomain (MD) structures, which leads to decreased magnetic stability and a reduction in the magnetic remanence per unit volume compared to SD grains. Small MD structures usually reside in a 'single vortex' structure (SV; Fig. 1b).

In addition to volume, the magnetic domain state of a crystal is strongly dependent on elongation; as particles become relatively more elongated the SD to MD transition size increases. Evans & McElhinny (1969) analytically calculated the first phase diagrams for domain state (SP, SD and MD) as a function of axial ratio [length versus grain-elongation axial-ratio (AR; short-axis/long-axis or width/length)] for individual magnetite particles. Such domain state phase diagrams are commonly used to assess the magnetic stability of magnetic crystals (Schumann *et al.* 2008; Lappe *et al.* 2011).

Using a slightly different approach, Butler & Banerjee (1975a,b) determined domain state phase diagrams from analytic calculations for both metallic iron and magnetite. Subsequently, for magnetite both the SP to stable SD transition size (Winklhofer *et al.* 1997) and the SD to MD transition size (Fabian *et al.* 1996; Newell & Merrill 1999; Witt *et al.* 2005; Muxworthy & Williams 2006) have been re-examined and revised for individual particles through application

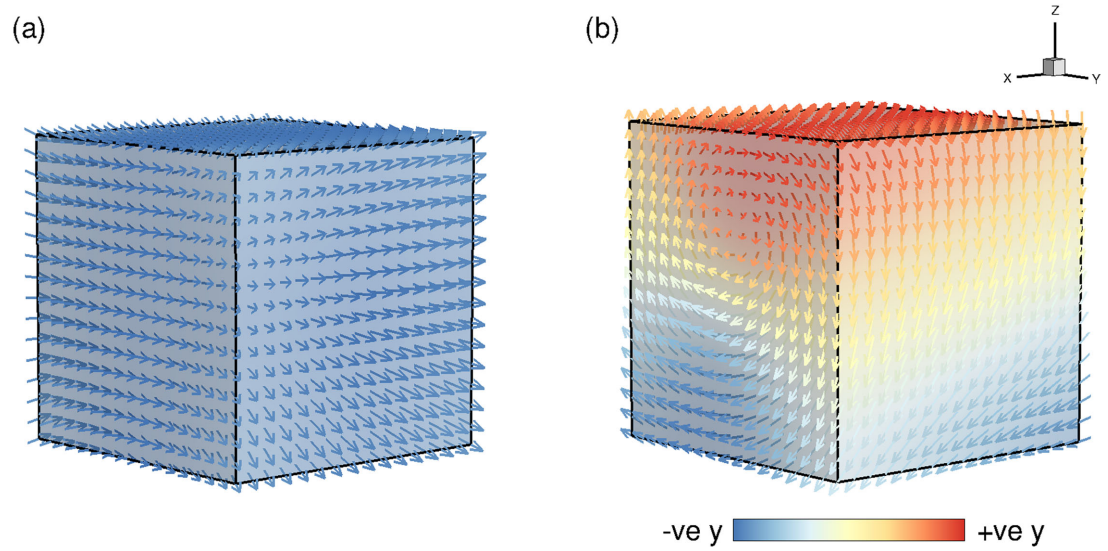

Figure 1. Domain states in cube-shaped grains of metallic iron at room temperature for a grain with an edge length of 25 nm: (a) single domain (flower state), and (b) single vortex state. In this paper, the term 'SD state' refers not just to homogeneous magnetization structures, but also to non-uniform domain structures as shown in (a), which are essentially SD-like with a degree of flowering toward the edges of the grain. In (a) and (b), the crystallographic ⟨100⟩ direction is aligned with the *x*-axis.

of the numerical micromagnetic equations of Brown (1963). Similar numerical calculations have recently been made for elongated greigite particles (Muxworthy *et al.* 2013).

The micromagnetic calculations for magnetite have shown that the earlier analytical calculations of by Evans & McElhinny (1969) and Butler & Banerjee (1975b) whilst state-of-the-art at the time, yield critical SD estimates significantly higher for elongated grains than the numerical calculations, for example, for cubic particles of magnetite the SD to MD transition was calculated by Butler & Banerjee (1975b) to be ∼76 nm and Muxworthy & Williams (2006) estimated it as ∼73 nm; however, for an AR of 0.4 this was ∼420 and ∼320 nm, respectively, a volume decrease of >50 per cent. In addition, crucially numerical models have shown that there is a range of grain sizes where both SD and SV structures can co-exist depending on the magnetic history; this was not predicted by traditional domain theory.

The estimate for the stable SD range for metallic iron by Butler & Banerjee (1975a) is still the main reference for our understanding the magnetic stability of iron/kamacite (Lappe *et al.* 2011; Gattacceca *et al.* 2014). In this paper, we present a modern numerical determination of the stable SD range for individual, elongated metallic iron: We determine both the SD to MD transition size, and the SP to SD size. All the magnetic properties required to model, say, $Fe_{0.95}Ni_{0.05}$ are not currently known; we therefore consider metallic iron.

2 THE SD/MD THRESHOLD SIZE

To determine the SD/MD threshold size as a function of elongation we employed the numerical algorithm described by Muxworthy & Williams (2006) and Muxworthy *et al.* (2013), except that we use the physical parameters for iron.

2.1 The micromagnetic algorithm

In the model, a grain is subdivided into a number of subcubes. Each subcube represents the averaged magnetization direction of many hundreds of atomic magnetic dipole moments. All of the subcubes have magnetic moments of equal magnitude, but the magnetization of the different subcubes can vary in direction. To determine the magnetic structures using this finite difference model, two approaches were considered; a combination of both a conjugate-gradient (CG) algorithm (Williams & Dunlop 1989) and a dynamic algorithm (Suess *et al.* 2002), and the CG algorithm alone. The reason for the combined approach is that the dynamic algorithm gives a more physical solution; however, it is computationally slow compared to the CG method. In the combined approach, we use the CG algorithm to rapidly generate a magnetic structure, which is then put into the dynamic solver as an initial estimate. This increases the efficiency of the algorithm by roughly an order of magnitude compared to the dynamic solver alone.

In the CG algorithm, the domain structure is calculated by minimizing the total magnetic energy E_{tot}, which is the sum of the exchange energy ($\propto$ the exchange constant A), the magnetostatic energy ($\propto {M_S}^2$, where M_S is the spontaneous magnetization) and the anisotropy energy ($\propto$the first magnetocrystalline anisotropy constant K_1) (Brown 1963). E_{tot} is calculated using a fast-Fourier transform (FFT) to give a local energy minimum (LEM) for the assemblage. The increased efficiency with which the demagnetizing energy can be calculated in Fourier space allows the high resolution needed to examine large elongated particles. The dynamic algorithm solves the dynamic Landau–Lifshitz–Gilbert equation. We used a finitely damped solver detailed by Brown *et al.* (1989). Instead of minimizing the energy, the solver minimizes the torque on each magnetic moment.

In this study, the following room-temperature values for metallic iron were used: $A = 2 \times 10^{-11}$ Jm^{-1} (Kittel 1949), $M_S = 1715 \times 10^3$ Am^{-1} (Dunlop & Özdemir 1997) and K_1 (cubic) $= 4.8 \times 10^4$ Jm^{-3} (Graham 1958). Butler & Banerjee (1975a) used values of: $A = 1 \times 10^{-11}$ Jm^{-1}, $M_S = 1720 \times 10^3$ Am^{-1} and $K_1 = 4.5 \times 10^4$ Jm^{-3}. The values used in this study are the ones now generally used in other micromagnetic studies of iron.

To model non-uniform structures, it is usually argued that it is necessary to have a minimum model resolution of two cells per

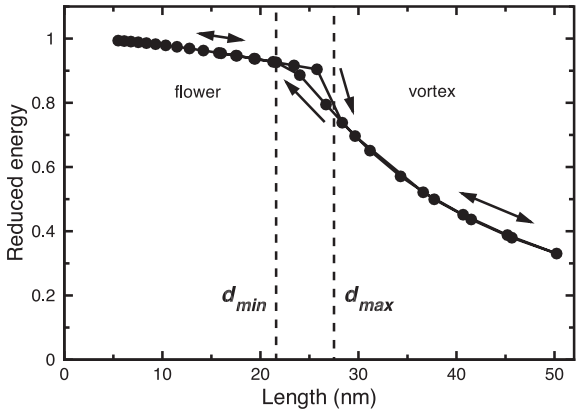

Figure 2. Magnetic energy density of a iron cube as a function of length for an initial SD configuration (*cf.* Fig. 1a) at room temperature. The grain size was gradually increased until the SD structure collapsed into a vortex structure (*cf.* Fig. 1b) at $d_{max}{}^{100} = 25$ nm. The size was then gradually decreased until a SD state formed at $d_{min}{}^{100} = 24$ nm. To maximize computational efficiency, the resolution was increased/decreased with each increase/decrease in size, and the domain structure was rescaled between each pair of calculations. The magnetic energy is normalized by that of a uniform SD structure of the same grain size.

exchange length (exchange length $= \sqrt{(A/K_d)}$, where $K_d = \mu_0 M_S{}^2/2$ and μ_0 is the permeability of free space (Rave *et al.* 1998). For iron at room temperature the exchange length is ∼3 nm; we used a minimum resolution of ∼1.5 nm at all times.

2.2 SD/MD critical sizes for individual elongated grains

There are several methods for determining the SD/MD critical size (d_0). Here, the unconstrained method is employed (Fabian *et al.* 1996; Witt *et al.* 2005; Muxworthy & Williams 2006). In this approach, a small grain, say 10 nm in length, with an initial SD structure (Fig. 1a) is gradually increased in size until the domain structure collapses to a SV (i.e. MD) state at d_{max} (Figs 1b and 2). The grain size is then decreased until the vortex structure becomes SD at d_{min} (Fig. 2).

The model calculations for a cube are shown in Fig. 2. The d_{min} and d_{max} values are interpreted to represent the lower and upper bounds, respectively, of a range of sizes where both SD and SV structures can co-exist. We have calculated d_{min} and d_{max} values as function of AR. For the most elongated grains, that is, AR < 0.4, d_{min} and d_{max} are poorly defined because the collapse is gradual and less abrupt. In such cases, the d_{min} and d_{max} values are estimated at the point where the reduced magnetization passes through 0.8 on the increasing/decreasing curves, where the reduced magnetization is the magnetic moment divided by the magnetic moment of an ideal SD grain.

The elongation induced anisotropy dominates the magnetocrystalline anisotropy for AR less than ∼0.9. For AR ∼1, the shape of the particle becomes important, that is, configurational anisotropy and surface roughness comes into effect (Williams *et al.* 2006), with cubes having different surface anisotropy energies compared to other shapes, etc. It has been numerically demonstrated (Shcherbakov & Sycheva 2001) that for magnetite spheres d_{min} and d_{max} converge and that the SD/SV critical size is close agreement with analytical calculations. However, perfect spheres are uncommon in nature and display magnetic characteristics distinct from all other shapes, even shapes with small variations from a sphere (Williams *et al.* 2011).

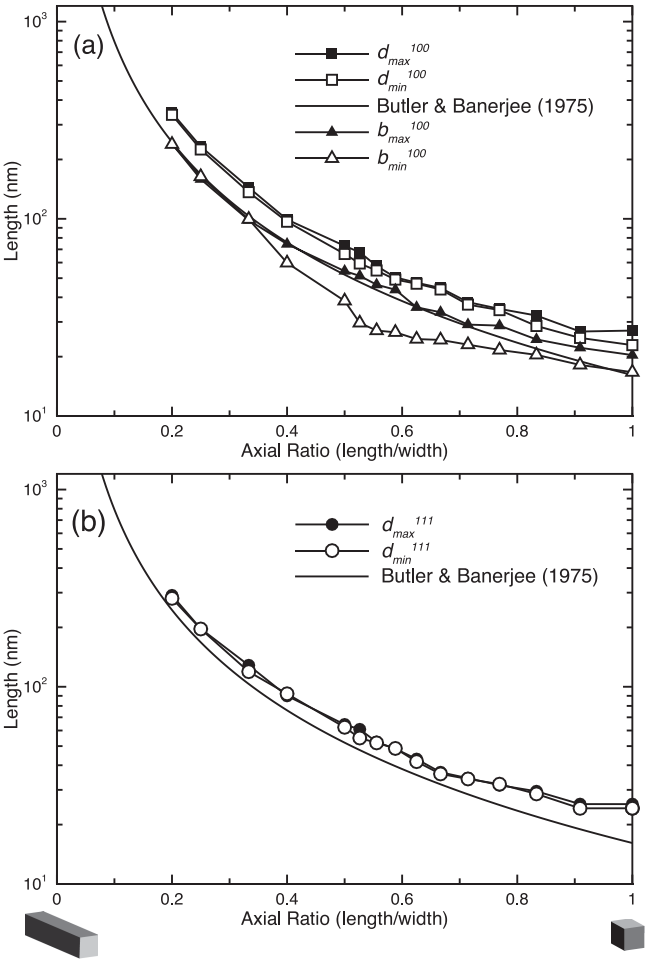

Figure 3. Critical SD to MD threshold lengths (maximum grain dimension) for individual iron particles as a function of axial ratio (AR). (a) Elongation along the ⟨100⟩ (easy anisotropy for $K_1 > 0$) direction, and (b) along the ⟨111⟩ (hard anisotropy for $K_1 > 0$) direction. Both d_{max} and d_{min} are shown. The lengths were determined using the method defined in Fig. 2. For highly elongated grains, that is, AR < 0.5, d_{max} and d_{min} are poorly defined. For these smaller values of AR, d_{max} and d_{min} were defined as the length where the reduced magnetization passed through 0.8 with increasing/decreasing grain size. AR $= 1$ is a cube and AR $= 0$ is an infinitely long rectangular cuboid. Also shown is the theoretical model of Butler & Banerjee (1975a), and in (a) $b_{max}{}^{100}$ and $b_{min}{}^{100}$ determined micromagnetically using the material parameters used by Butler & Banerjee (1975a). For clarity for AR $= 1$: $d_{max}{}^{100}$ ∼27 nm, $d_{min}{}^{100}$ ∼23 nm, $b_{max}{}^{100}$ ∼20 nm, $b_{min}{}^{100}$ ∼17 nm, $d_{max}{}^{111}$ ∼25 nm and $d_{min}{}^{111}$ ∼24 nm.

In addition to calculating d_{min} and d_{max} as a function of AR, we have considered the relationship between the relative orientation of the cubic magnetocrystalline anisotropy and the particle elongation. We model two extreme cases: first, where the elongation is in the easy direction (i.e. ⟨100⟩ axes for $K_1 > 0$) (yielding $d_{min}{}^{100}$ and $d_{max}{}^{100}$) and second where it is in the hard direction ($d_{min}{}^{111}$ and $d_{max}{}^{111}$). In the scenario with elongation along the easy direction, the magnetocrystalline anisotropy enhances the shape effect. In contrast, when the elongation is along the hard direction, the magnetocrystalline anisotropy competes with the shape effect.

Generally $d_{min}{}^{100}$, $d_{max}{}^{100}$, $d_{min}{}^{111}$ and $d_{max}{}^{111}$ increase as AR decreases (Fig. 3). In Fig. 3, the *y*-axis is the particle length as used by Butler & Banerjee (1975a), rather than the mean diameter as used by Witt *et al.* (2005). Use of the particle length enables easier comparison with the results of Butler & Banerjee (1975a), but mixes

the effects of shape and volume. The d_{max}^{100} value is the largest of the four estimates for all values of AR. Orienting the magnetization along the easy axis enhances the effect of elongation, while orientation along the hard direction increases curling of the magnetization at the edges of the grains, which breaks symmetry, and encourages nucleation of vortex states and decreases d_0. As AR is reduced, the difference between d_{min}^{100} and d_{max}^{100}, and d_{min}^{111} and d_{max}^{111} decreases as the shape anisotropy increasingly dominates the magnetocrystalline anisotropy.

For comparison, the calculated results of Butler & Banerjee (1975a) are depicted in Fig. 3. Our micromagnetic estimates of the SD/MD threshold size are higher than those obtained from the analytical results of Butler & Banerjee (1975a). For example, for a cubic grain, the micromagnetic model gives an estimate of ~24 nm (d_{min}^{100}) compared to ~17 nm from of Butler & Banerjee (1975a). This trend was opposite to that found for magnetite (Muxworthy & Williams 2006), where the micromagnetic calculation produced lower estimates than the analytical one. To examine whether the difference is due to the method of calculation or the slightly different choice of material constants, we micromagnetically calculated d_{min}^{100} and d_{max}^{100} (b_{min}^{100} and b_{max}^{100}) for the parameters used by Butler & Banerjee (1975a) detailed above in Section 2.1 (Fig. 3a). It is seen that b_{max}^{100} is similar to the original calculation of Butler & Banerjee (1975a) for AR < 0.7; for AR $= 1$, $b_{max}^{100} \sim 20$ nm. For AR $= 1$, $b_{min}^{100} \sim 17$ nm, very close to the estimate of Butler & Banerjee (1975a); clearly the choice of input parameters is critical.

While the results differ to those of Butler & Banerjee (1975a), the micromagnetic results of this study are in good agreement with the threshold size of ~23 nm determined experimentally or bulk samples containing symmetric iron particles (Kneller & Luborsky 1963), and ~28 nm determined micromagnetically for cubes of iron (Snoeck *et al.* 2008).

The difference between d_{min}^{100} and d_{max}^{100}, and d_{min}^{111} and d_{max}^{111}, is relatively smaller than for magnetite (Muxworthy & Williams 2006) and greigite Muxworthy *et al.* (2013). For example, for magnetization along the magnetocrystalline easy axis, for AR $= 1$ for magnetite ($K_1 < 0$), d_{min}^{100} and d_{min}^{111} are ~61 and ~67 nm, respectively (Muxworthy & Williams 2006), compared to iron; d_{min}^{100} and d_{min}^{111} are ~23 and ~24 nm, respectively.

3 THE SP/SD BOUNDARY

SD grains below a certain critical volume (the blocking volume, v_b) are magnetically unstable and have SP behaviour. For an individual particle the relaxation time t_m, is given by Néel (1949):

$$t_m = \tau_0 \exp(E_A/kT), \quad (1)$$

where E_A is the anisotropy energy barrier, k is Boltzmann's constant, T is the temperature and τ_0 is the atomic reorganization time (~10^{-9}, Worm 1998). The relaxation time t_m can be a few nanoseconds for SP particles that undergo thermal relaxation during laboratory experiments to billions of years for stable SD particles in geological and planetary samples. This equation is strictly for a system with only two possible states; however, in elongated grains this is the case. For symmetrical samples with higher order magnetocrystalline anisotropy, small errors will occur in blocking volume estimations.

We directly determine the SP/SD threshold from the energy barrier (eq. 1) from the anisotropy energy surface. The model includes both the cubic magnetocrystalline anisotropy of iron plus a 'shape anisotropy', which is calculated in the magnetostatic energy term.

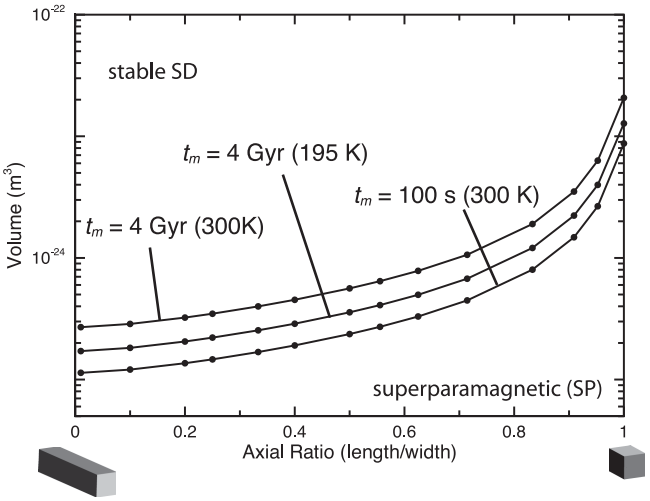

Figure 4. Blocking volume curves on a volume versus axial ratio for single crystals of iron. Grain elongation is in the ⟨100⟩ direction. Two relaxation times for t_m at 300 K are shown: 100 s and 4 Gyr, the other is for $t_m = 4$ Gyr at 195 K. The blocking volumes were determined directly from eq. (1).

Values of $t_m = 100$ s and 4 Gyr at 300 K are plotted against grain volume in Fig. 4. The longer timescale was chosen because of potential interests in magnetic stabilities over the age of the Earth, while the shortest timescale demonstrates variability in t_m. Additionally, as the surface temperature of asteroids is ~100–200 K, we also determine $t_m = 4$ Gyr, using data for iron at 195 K (Graham 1958, 1960). For single crystals, v_b decreases with increasing elongation (decreasing AR), in agreement with calculations for various minerals (Muxworthy & Williams 2009; Newell 2009; Muxworthy *et al.* 2013). Decreasing either the temperature or t_m decreases v_b, but the trend is similar, just shifted to lower values. The room-temperature SP/SD transition results (Fig. 4) are very similar to those of Butler & Banerjee (1975a), except for AR > 0.9, where Butler & Banerjee (1975a) calculated the SP/SD transition separately for shape and magnetocrystalline anisotropy controlled particles. In contrast, in this paper the combined anisotropy was used in the calculation.

4 DOMAIN-STATE PHASE DIAGRAM

We have constructed a domain-state phase diagram for elongated metal iron particles (Fig. 5), using $t_m = 100$ s and 4 Gyr at 300 K calculations for the SP/SD transition, and the d_{min}^{100} and d_{max}^{100} data. The micromagnetic models are theoretically more accurate than previous analytical models (Butler & Banerjee 1975a), but the choice of input material parameters is also important.

In agreement with Butler & Banerjee (1975a), for long t_m (~4 Gyr) at 300 K, there is a direct SP to MD transition for near equate iron particles. This paper finds the transition to be for AR $>$ 0.95, in contrast Butler & Banerjee (1975a) predicted this transition for AR > 0.8.

4.1 Comparison with electron holography data

Plotted in Fig. 5 are domain-state observational data for 40 olivine-hosted FeNi (kamacite) particles from Lappe *et al.* (2011), determined by the advanced transmission electron microscopy technique of off-axis electron holography. Electron holography directly images the magnetisation on nanometric scales allowing the identification

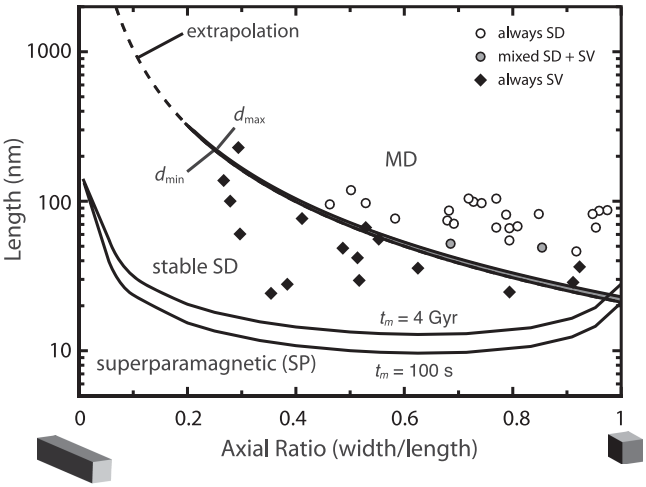

Figure 5. Stable SD grain size ranges for individual particles of metallic iron. Grain elongation is in the ⟨100⟩ direction. The grey area between d_{max} and d_{min} indicates the range where both SD and SV (MD) states are possible. For the SP/SD transition lines are for t_m = 100 s and 4 Gyr at 300 K. Published domain-state observational data for 40 Fe–Ni particles in synthetic 'dusty olivines' are also plotted (Lappe *et al.* 2011). Lappe *et al.* (2011) examined each particle more than once, and determined whether they were always SD, always SV (MD) or displayed mixed states. Increasing levels of Ni, will increase the SD to MD transition size.

of domain state, that is, SD-like or SV-like (Dunin-Borkowski *et al.* 1998). Lappe *et al.* (2011) examined each particle more than once, and determined whether they were always SD, always SV or displayed mixed states; there was little indication of inter-grain magnetostatic interaction. The samples were synthetic 'dusty-olivines' produced from natural olivine crystals from Iceland.

Generally the SD states plot within the theoretical SD region, and the SV states within the theoretical MD region; importantly, the micromagnetic model better describes the data than the model of Butler & Banerjee (1975a). There are a few particles that do not agree with the numerical results, however, there are three possible causes for this: (1) The dimensions of the particles were determined from 2-D images, not tomography, therefore the thickness (and volume) of the particles is not accurately known, that is, there is a large degree of error as to the exact position of the particles on the domain state plot (Fig. 5). (2) The amount of nickel in the Fe–Ni is unknown; the model assumes stoichiometric iron; as the Ni content increases from Fe to $Fe_{0.95}Ni_{0.05}$ in the Fe–Ni system, M_S increases slightly, whilst A and K_1 decrease slightly (Tarasov 1939; Bozorth 1951). This will cause the SD/MD boundary limit to increase slightly. (3) It is becoming increasingly realised that the interpretation of electron holography images is not always straightforward, and commonly it is necessary to use micromagnetic solutions to interpret the images (Bryson *et al.* 2013; Almeida *et al.* 2014); Lappe *et al.* (2011) did not do this as this has only recently become standardised.

5 CONCLUSIONS

We have calculated and constructed the first domain-state phase diagram using a 3-D micromagnetic algorithm for elongated iron particles (Fig. 5). The predicted SD to MD transition size is larger than in the previous calculations of Butler & Banerjee (1975a). This difference has been shown to be partially related to the choice of material parameters used. For AR = 1 the SD to MD transition size agrees well with previous micromagnetic results (Snoeck *et al.* 2008). The analytically determined SP to SD transition is similar to that of Butler & Banerjee (1975a), except for equant grains as this paper calculated the transition using a combination of shape and magnetocrystalline anisotropy. Direct observations of the domain state of FeNi particles by electron holography (Lappe *et al.* 2011), agree better with the new domain-state phase diagram (Fig. 5) than that of Butler & Banerjee (1975a). Increasing levels of Ni, will increase the SD to MD transition size.

ACKNOWLEDGEMENTS

This work was funded by STFC consolidated grant ST/J001260/1.

REFERENCES

Almeida, T.P., Kasama, T., Muxworthy, A.R., Williams, W., Nagy, L. & Dunin-Borkowski, R.E., 2014. Observing thermomagnetic stability of non-ideal magnetite particles: good paleomagnetic recorders? *Geophys. Res. Lett.,* **41**(20), 7041–7047.

Bozorth, R.M., 1951. *Ferromagnetism,* Van Nostrand.

Brown, P.N., Byrne, G.D. & Hindmarsh, A.C., 1989. VODE: a variable coefficient ODE solver, *SIAM J. Sci. Stat. Comput.,* **10,** 1038–1051.

Brown, W.F. Jr., 1963. *Micromagnetics,* John Wiley.

Bryson, J.F.J., Kasama, T., Dunin-Borkowski, R.E. & Harrison, R.J., 2013. Ferrimagnetic/ferroelastic domain interactions in magnetite below the Verwey transition. Part II: micromagnetic and image simulations, *Phase Trans.,* **86,** 88–102.

Butler, R.F. & Banerjee, S.K., 1975a. Single-domain grain size limits for metallic iron, *J. geophys. Res.,* **80,** 252–259.

Butler, R.F. & Banerjee, S.K., 1975b. Theoretical single-domain grain size range in magnetite and titanomagnetite, *J. geophys. Res.,* **80,** 4049–4058.

Dunin-Borkowski, R.E., McCartney, M.R., Frankel, R.B., Bazylinski, D.A., Pósfai, M. & Buseck, P.R., 1998. Magnetic microstructure of magnetotactic bacteria by electron holography, *Science,* **282,** 1868–1870.

Dunlop, D.J. & Özdemir, Ö., 1997. *Rock Magnetism: Fundamentals and Frontiers,* Cambridge Univ. Press.

Evans, M.E. & McElhinny, M.W., 1969. The origin of stable remanence in magnetite-bearing igneous rocks, *J. Geomag. Geoelect.,* **21,** 757–773.

Fabian, K., Kirchner, A., Williams, W., Heider, F., Leibl, T. & Huber, A., 1996. Three-dimensional micromagnetic calculations for magnetite using FFT, *Geophys. J. Int.,* **124,** 89–104.

Garrick-Bethell, I. & Weiss, B.P., 2010. Kamacite blocking temperatures and applications to lunar magnetism, *Earth planet. Sci Lett.,* **294,** 1–7.

Gattacceca, J., Suavet, C., Rochette, P., Weiss, B.P., Winklhofer, M., Uehara, M. & Friedrich, J.M., 2014. Metal phases in ordinary chondrites: Magnetic hysteresis properties and implications for thermal history, *Meteor. planet. Sci.,* **49,** 652–676.

Graham, C.D., 1958. Magnetocrystalline anisotropy constants of iron at room remperature and below, *Phys. Rev.,* **112,** 1117–1120.

Graham, C.D., 1960. Temperature dependence of anisotropy and saturation magnetization in iron and iron-silicon alloys, *J. appl. Phys.,* **31,** 150S–160S.

Kittel, C., 1949. Physical theory of ferromagnetic domains, *Rev. Modern Phys.,* **21,** 541–583.

Kneller, E.F. & Luborsky, F.E., 1963. Particle size dependence of coercivity and remanence of single-domain particles, *J. appl. Phys.,* **34,** 656–658.

Lappe, S. *et al.*, 2011. Mineral magnetism of dusty olivine: a credible recorder of pre-accretionary remanence, *Geochem. Geophys. Geosyst.,* **12,** Z1235, doi:10.1029/2011GC003811.

Lappe, S., Harrison, R.J., Feinberg, J.M. & Muxworthy, A., 2013. Comparison and calibration of nonheating paleointensity methods: a case study using dusty olivine, *Geochem. Geophys. Geosyst.,* **14,** 2143–2158.

Muxworthy, A.R. & Williams, W., 2006. Critical single-domain/multidomain grain sizes in non-interacting and interacting elongated magnetite particles: Implications for magnetosomes, *J. geophys. Res.,* **111,** B12S12, doi:10.1029/2006jb004588.

Muxworthy, A.R. & Williams, W., 2009. Critical superparamagnetic/single-domain grain sizes in interacting magnetite particles: implications for magnetosome crystals, *J. R.. Soc. Inter.,* **6,** 1207–1212.

Muxworthy, A.R., Williams, W., Roberts, A.P., Winklhofer, M., Chang, L. & Pósfai, M., 2013. Critical single domain grain sizes in interacting greigite particles: implications for magnetosome crystals, *Geochem. Geophys. Geosyst.,* **14,** doi:10.1002/2013GC004973.

Néel, L., 1949. Influence des fluctuations thermiques sur l'aimantation de grains ferromagnétiques très fins, *Comp. Ren. Heb. Séan. Acad. Sci.,* **228,** 664–666.

Newell, A.J., 2006. Superparamagnetic relaxation times for mixed anisotropy and high energy barriers with intermediate to high damping: 1. Uniaxial axis in a ⟨001⟩ direction, *Geochem. Geophys. Geosyst.,* **7,** Q03016, doi:10.1029/2005GC001146.

Newell, A.J., 2009. Transition to superparamagnetism in chains of magnetosome crystals, *Geochem. Geophys. Geosyst.,* **10,** Q11Z08, doi:10.1029/2009GC002538.

Newell, A.J. & Merrill, R.T., 1999. Single-domain critical sizes for coercivity and remanence, *J. geophys. Res.,* **104,** 617–628.

Pechersky, D.M., Markov, G.P., Tsel'movich, V.A. & Sharonova, Z.V., 2012. Extraterrestrial magnetic minerals, *Iz. Phys. Solid Earth,* **48,** 653–669.

Rave, W., Fabian, K. & Hubert, A., 1998. Magnetic states of small cubic particles with uniaxial anisotropy, *J. Magn. Magn. Mater.,* **190,** 332–348.

Schumann, D. *et al.*, 2008. Gigantism in unique biogenic magnetite at the Paleocene-Eocene thermal maximum, *Proc. Natl. Acad. Sci. USA,* **105,** 17 648–17 653.

Shcherbakov, V.P. & Sycheva, N.K., 2001. Numerical modeling of the domain structure in magnetite grains of submicron sizes, *Iz. Phys. Solid Earth,* **37,** 334–344.

Snoeck, E., Gatel, C., Lacroix, L.M., Blon, T., Lachaize, S., Carrey, J., Respaud, M. & Chaudret, B., 2008. Magnetic configurations of 30 nm iron nanocubes studied by electron holography, *Nano Letters,* **8,** 4293–4298.

Suess, D., Tsiantos, V., Schrefl, T., Fidler, J., Scholz, W., Forster, H., Dittrich, R. & Miles, J.J., 2002. Time resolved micromagnetics using a preconditioned time integration method, *J. Magn. Magn. Mater.,* **248,** 298–311.

Tarasov, L.P., 1939. Ferromagnetic anisotropy of low nickel alloys of iron, *Phys. Rev.,* **56,** 1245–1246.

Uehara, M. & Nakamura, N., 2006. Experimental constraints on magnetic stability of chondrules and the paleomagnetic significance of dusty olivines, *Earth planet. Sci Lett.,* **250,** 292–305.

Weiss, B.P., Gattacceca, J., Stanley, S., Rochette, P. & Christensen, U.R., 2010. Paleomagnetic records of meteorites and early planetesimal differentiation, *Space Sci. Rev.,* **152,** 341–390.

Williams, W. & Dunlop, D.J., 1989. Three-dimensional micromagnetic modelling of ferromagnetic domain structure, *Nature,* **337,** 634–637.

Williams, W., Muxworthy, A.R. & Paterson, G.A., 2006. Configurational anisotropy in single-domain and pseudosingle-domain grains of magnetite, *J. geophys. Res.,* **111,** doi:10.1029/2006jb004556.

Williams, W., Muxworthy, A. & Evans, M., 2011. A micromagnetic investigation of magnetite grains in the form of Platonic polyhedra with surface roughness, *Geochem. Geophys. Geosyst.,* **12,** Q10Z31, doi:10.1029/2011GC003560.

Winklhofer, M., Fabian, K. & Heider, F., 1997. Magnetic blocking temperatures of magnetite calculated with a three-dimensional micromagnetic model, *J. geophys. Res.,* **102,** 22 695–22 709.

Witt, A., Fabian, K. & Bleil, U., 2005. Three-dimensional micromagnetic calculations for naturally shaped magnetite: octahedra and magnetosomes, *Earth planet. Sci Lett.,* **233,** 311–324.

Worm, H.-U., 1998. On the superparamagnetic-stable single domain transition for magnetite, and frequency dependence of susceptibility, *Geophys. J. Int.,* **133,** 201–206.